IEEE Access
Multidisciplinary : Rapid Review : Open Access Journal

Received June 19, 2021, accepted July 14, 2021, date of publication July 20, 2021, date of current version July 26, 2021.

Digital Object Identifier 10.1109/ACCESS.2021.3098562

A State-Space Approach for Tracking Doppler Shifts in Radio Inter-Satellite Links

PEDRO PEDROSA[1], DANIEL CASTANHEIRA[1], ADÃO SILVA[2], RUI DINIS[3], (Senior Member, IEEE), AND ATÍLIO GAMEIRO[2]

[1]Instituto de Telecomunicações, Universidade de Aveiro, 3810-193 Aveiro, Portugal
[2]DETI, Instituto de Telecomunicações, Universidade de Aveiro, 3810-193 Aveiro, Portugal
[3]DEE, FCT, Instituto de Telecomunicações, Universidade Nova de Lisboa, 2825-149 Costa da Caparica, Portugal

Corresponding author: Pedro Pedrosa (pmfopedrosa@av.it.pt)

This work was supported in part by the European Regional Development Fund (FEDER), through the Competitiveness and Internationalization Operational Program (COMPETE 2020) of the Portugal 2020 framework, in part by the Regional OP Centro under Grant POCI-01-0145-FEDER-030588, in part by the Regional OP Lisboa under Grant Lisboa-01-0145-FEDER-03058, and in part by the FCT/MEC through national funds under Project MASSIVE5G (PTDC/EEI-TEL/30588/2017) and Project UIDB/50008/2020-UIDP/50008/2020.

ABSTRACT The high Doppler effects in satellite communications make the equivalent channels fast varying, which leads to channel estimation difficulties and the need for high channel estimation overheads. In this paper we propose a state-space approach for tracking channel variations for satellite links with high Doppler frequency shifts. We consider the communication between satellite links where a multi-antenna receiving satellite is connected to several transmitting satellites, which can have substantially different Doppler drifts. The proposed channel tracking technique follows the individual Doppler drifts for the different satellites. Finally, our performance results indicate that the proposed channel tracking is able to cope with strong Doppler drifts, without the need for high channel estimation overheads, making it a promising technique for future systems using satellite mega-constellations.

INDEX TERMS Channel tracking, Doppler effects, extended Kalman filters, satellite communications.

I. INTRODUCTION

The integration of non-terrestrial networks (NTN) into 5G as specified by the 3GPP [1]–[4] represents the first systematic effort to include satellite-based networks into the standard of a new mobile communications generation. In fact, there are two approaches to effectively integrating satellites into the cellular network: backhaul and direct access.

Backhaul, which is already well established [5], uses satellites to connect cellular base stations in remote areas to the cellular network, if necessary without any further infrastructure. It requires, however, that both the satellite and the user terminal are connected to a cellular base station. Direct access, conversely, is supported on direct communication between the satellite and the user terminal. This means access to the 5G network at all times everywhere, even when a base station is not available. Moreover, network architectures in which the satellite itself, either fully or partially, serves as the base station are also possible [6].

The associate editor coordinating the review of this manuscript and approving it for publication was Di Zhang.

This integration means that not only terrestrial cellular networks can count on satellites to support truly ubiquitous coverage, but also that the satellite industry has here an opportunity to expand its business. In fact, the deployment of mega-constellations counting several thousands satellites is currently underway (see [7] and references within), where low-earth orbits (LEO)s are preferred to the higher altitude medium-earth orbits (MEO)s or even the geostationary-earth orbits (GEO)s due to their reduced delay, path loss, and satellite production and launching costs [8]–[11]. Moreover, since propagation loss is small in LEOs, it is possible to realize practical communication systems with small satellites and earth stations. In addition, non-geostationary LEO satellites have access to earth stations located in high latitude areas such as the polar regions, thus contributing to a truly global coverage.

Both LEO and GEO satellites communications can benefit from duplex communications [12]. For GEO satellites pointing to a fixed ground station, the Doppler shift is not expected to introduce any critical issue, since the transmitter and receiver are static, but the very large propagation delays might have a strong impact on the PHY/MAC procedures.

On the other hand, for LEO satellites the propagation delays are much smaller, and real-time duplex communication channels can be more easily amenable.

Though the non-geostationary LEO satellite systems have attractive features, they also present some particular challenges [12]. Being one of the most important issues the frequency Doppler shift. Since the non-geostationary satellites change their relative positions to earth stations, the signals suffer from Doppler shifts whose value and drift rate are very large compared with that in the systems with geostationary satellites or in the terrestrial systems.

Various Doppler shift estimation algorithms have been proposed for the LEO satellite communication systems. An early characterization of the Doppler shift in the non-geostationary LEO satellite communication systems is found in [13] where the satellite communicates with a fixed terminal on Earth. Similarly, [14]–[16] exploit the fact that the relative angular velocity between the satellite and the Earth is constant to characterize the Doppler shift as a function of the time and the maximum elevation angle of the LEO satellite. These approaches, however, consider that the satellite speeds and directions are known to the Earth terminal and that the Earth terminal is fixed while in our setup the satellites speeds and directions are not known to the terminal and the terminal itself is moving. Moreover, the efficiency of Doppler tracking techniques based on satellite trajectory is directly linked to the accuracy of the Doppler characterization curves, which are typically obtained using approximations [14]. Even if these approximations do not compromise the value of such approaches, the presence of inaccuracies on the model means that they are not able to fully compensate the detrimental presence of Doppler shifts. The presence of residual Doppler shifts motivates the proposal of different Doppler tracking techniques supported on alternative approaches, eventually complementing the satellite trajectory-based approaches.

The use of Kalman-based techniques for synchronization purposes is not new to the literature (see [17], and references within, or the more recent work [18]) and some of these techniques were even considered for space applications, particularly as a mean to track highly dynamic GPS signals [19]–[22]. The use of Kalman filters for tracking Doppler shifts in broadband radio inter-satellite communications appears in [23]–[25]. Particularly in [25], the tracking of the Doppler shift is done using a prime synchronizing signal while resorting to the Kalman filter as an additional measure to further stabilize the tracking procedure. In [23], a distributed MIMO system emulating virtual antenna arrays is considered where a reference signal is sent by the master node to the cooperative nodes and a Kalman filter is used to track the Doppler shift. However, the tracking procedure takes place at the transmitter, which sends a pre-compensated signal. Finally, in [24] an auto-correlation function is used to obtain an initial estimate of the frequency offset and then a Kalman filter to optimize this estimate. The Kalman filter is shown to improve the stability of estimated frequency offset and track the time-varying frequency offset. However, this approach is limited to scenarios with a single satellite link or multiple satellite links with identical Doppler shifts.

An extensive analysis of the power budgets for satellite communications supporting ground communications and inter-satellite links is provided in [26]. Although focused solely on CubeSats, their analysis is particularly valuable since CubeSats have very limited power resources. This means that the results obtained for them may eventually lower bound larger satellites, potentially provided with more resources (e.g., larger solar-panels and batteries). The link budget analysis of [26] assumes a transmit power level of 15 dBm (about 31.62 mW) for the satellite, corresponding to a Universal Software Radio Platform (USRP) B-200 with no additional amplifiers, and a transmit power level of 50 dBm (100 W) for the ground station. The latter value, however, assumes that the ground station transmit power is only limited by its operating license, which is something that is not aligned with our scenario where the ground station is a mobile, eventually, handheld device. Thus, a more realistic assumption would be less than 0.5 W transmit power for handheld devices, 2 W for portable devices (e.g., laptop or notebook), and 10 W for vehicular terminals [27].

Power constraints and efficient amplification requirements favours single-carrier (SC) modulations instead of the more popular OFDM schemes. Notably, SC combined with frequency-domain equalization (SC-FDE) if dealing with time-dispersive channels [28]–[31]. In fact, for terrestrial mobile communications SC-FDE has been advocated as a particularly promising scheme for the uplink (i.e., when the communication signal goes from the mobile terminal to the base station) [32]. This is due to the fact that SC-FDE schemes have simpler transmitters, lower peak-to-average power ratio (PAPR), and increased robustness to carrier-frequency offset (CFO) compared to OFDM. This makes SC-FDE schemes also an interesting candidate for satellite communications.

This work proposes a state-space approach for tracking channel variations for satellite links with high Doppler frequency shifts. With the proposed approach, we aim at solving the problem of Doppler shifts in both space-to-space and earth-to-space communications. Where in the latter, the earth device is assumed to be mobile. As far as we know, our work is the first to consider a mobile communication system architecture where a multi-input multi-output (MIMO) receiver satellite (or earth receiver) is connected to multiple transmitter satellites with high Doppler frequency shifts associated. If the Doppler shifts associated to each different satellite link were identical, this would be similar to scenario with a carrier frequency offset (CFO) [24]. However, the different velocities of the satellites lead to different Doppler shifts making their estimation and compensation much more complex. Typically, the estimation overheads increase with the Doppler shift [33], and the number of simultaneous transmissions, while in our case they only increase with the number of simultaneous transmissions.

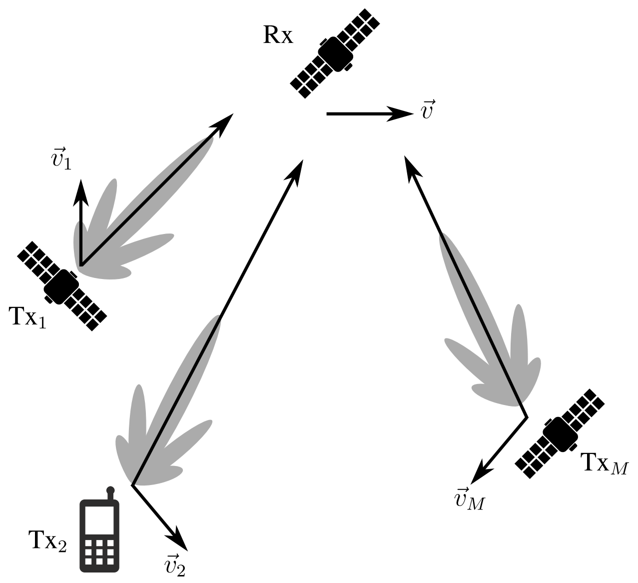

FIGURE 1. Transmission scenario with both space-to-space and earth-to-space communications.

This work is organized as follows. After this introductory section we present the transmission scenario in Sec. II, the frequency-domain channel equalization and estimation in Sec. III, and the Doppler frequency shift tracking in Sec. IV. Finally, we present the performance results in Sec. V, and the conclusions in Sec. VI.

The notation used in this work is the following. Transpose, conjugate, and conjugate-transpose are denoted by $(\cdot)^\top$, $(\cdot)^*$, and $(\cdot)^\dagger$, respectively. Operator $\angle\{\cdot\}$ returns the phase of a complex number; DFT$\{\cdot\}$ denotes the discrete Fourier transform and IDFT$\{\cdot\}$ its inverse. The matrix $\mathbf{I}_M$ is an $(M \times M)$ identity matrix, and $\mathbf{1}_M$ is a column vector with M elements. Operator $\otimes$ is the Kronecker matrix product.

II. TRANSMISSION SCENARIO

Consider the transmission scenario depicted in Fig. 1 where M satellites (or mobile earth devices), each with T antennas, transmit a radio signal to a receiver satellite with R antennas. The receiver satellite moves with velocity $\vec{v}$, and the ith transmitter satellite (or earth device) with velocity $\vec{v}_i$. For the sake of simplicity we consider line-of-sight (LoS) conditions, which is the typical situation in satellite-to-satellite communications [16], [24]. For satellite to ground communications, we can have multipath propagation effects, especially when the ground antennas are not too directive.

Consider the Doppler shift $f_D^{(i)} = \frac{f_c}{c}\vec{v}_i'$, where f_c is the carrier frequency, c the speed of light, and $\vec{v}_i'$ the relative speed between the ith transmitter and the receiver. Now, assume an angle-of-departure (AoD) θ_i formed by the velocity vector $\vec{v}_i$ of the transmitter satellite Tx_i and the LoS path, and an angle-of-arrival (AoA) ϑ_i formed by the velocity vector $\vec{v}$ of the receiver satellite Rx and the LoS path (see Fig. 2) then results that the Doppler drift at the receiver caused by Tx_i is

$$f_D^{(i)} = \frac{f_c}{c}\left(|\vec{v}_i|\cos(\theta_i) - |\vec{v}|\cos(\vartheta_i)\right). \tag{1}$$

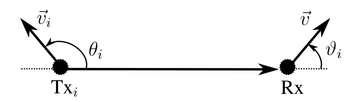

FIGURE 2. Relation between the AoD θ_i and the AoA ϑ_i.

Considering that we have LoS communication only, and that the radio channel between the transmitter satellite Tx_i and the rth antenna element of the receiver satellite is characterized by a path coefficient $\alpha^{(r,i)} \in \mathbb{C}$, and a path delay $\tau^{(i)}$, results that the baseband channel impulse response (CIR) is given by

$$h^{(r,i)}(t, t_0) = \alpha^{(r,i)}(t_0)\delta(t - \tau^{(i)}(t_0)). \tag{2}$$

Assuming that the path delay is slowly varying,[1] i.e., $\tau^{(i)}(t_0) \approx \tau^{(i)}$ with $\tau^{(i)} \triangleq \tau^{(i)}(0)$, and that $\alpha^{(r,i)}(t_0) \approx \alpha^{(r,i)}e^{j2\pi f_D^{(i)} t_0}$ with $\alpha^{(r,i)} \triangleq \alpha^{(r,i)}(0)$, and $f_D^{(i)}$ the Doppler frequency shift (1), then (2) can be written as

$$h^{(r,i)}(t, t_0) = \alpha^{(1,i)}e^{j2\pi[f_D^{(i)}t_0 + \frac{d}{\lambda}(r-1)\cos(\vartheta_i)]}\delta(t - \tau^{(i)}), \tag{3}$$

where $\alpha^{(1,i)}$ denotes the path coefficient associated to Tx_i and the first antenna element of the receiver,[2] d the separation between the array elements, and λ the radio signal wavelength. Notice that, each AoA ϑ_i should be different (i.e., $|\vartheta_i - \vartheta_{i'}| > 0$) in order to ensure that we are able to separate the different incoming signals at the receiver.[3]

III. CHANNEL EQUALIZATION AND ESTIMATION

This section deals with the equalization and estimation of the satellite radio channel, which we are assuming to happen in the frequency-domain.

A. FRAME STRUCTURE

Consider Fig. 3 where we depict the proposed frame structure. Particularly, the frame starts with one training block[4] (TB) from Tx_1, followed by a TB from Tx_2, and so forth until Tx_M transmits its TB. This is done twice.

During this training stage, while one satellite is transmitting the other satellites are silent. So the training stage is orthogonal in time. Notice that the training stage allows to obtain an estimate $\hat{f}_D^{(i)}$ of the Doppler shift. Accordingly,

$$\hat{f}_\text{D}^{(i)} = \frac{1}{2\pi\Delta T} \cdot \frac{1}{R}\sum_{r=1}^{R}\Phi^{(r,i)} \tag{4}$$

with

$$\Phi^{(r,i)} = \angle\left\{\hat{h}^{(r,i)}(t, t_0)\left(\hat{h}^{(r,i)}(t, t_0 - \Delta T)\right)^*\right\} \tag{5}$$

[1] This is motivated by the fact that the tap amplitudes change at a much slower rate than its phase in the presence of the Doppler effects associated to satellite communications.

[2] We consider a uniform linear array (ULA) but other array geometries could be examined.

[3] Signals from satellites coming from the same direction need to be separated by other means, such as different bands or time slots.

[4] Notice that the training block can be smaller than the data block.

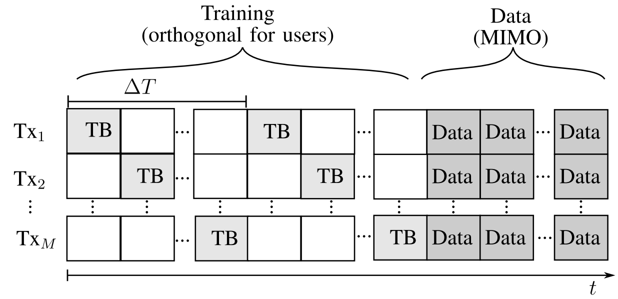

FIGURE 3. Proposed frame structure.

where $\hat{h}^{(r,i)}(t)$ is the estimate of the CIR obtained during the training stage (see Sec. III-B), and $|2\pi f_D^{(i)}\Delta T| < \pi$. The variance of the estimate is $\sigma^2_{\hat{f}_D} \propto \frac{1}{\Delta T}$.

Notice that, the estimate of the CIR results from applying the IDFT to the *de facto* estimated CFR after an appropriate sampling process, i.e., $\{\hat{h}_n^{(r,i)};\ n = 0, 1, \ldots, N-1\} = \mathrm{IDFT}\{\hat{H}_k^{(r,i)};\ k = 0, 1, \ldots, N-1\}$.

B. CHANNEL ESTIMATION WITH TRAINING

Assume that only Tx_i is active and that the transmitted signal is a known training block $\{S_k^{\mathrm{TB}\,(i)};\ k = 0, 1, \ldots, N-1\}$ in the frequency-domain, and that the signal received at the rth antenna element is $\{Y_k^{(r)};\ k = 0, 1, \ldots, N-1\}$, also in the frequency-domain. Accordingly, an estimate of the channel frequency-response (CFR) associated to the rth antenna element of the receiver and ith transmitter satellite is readily available doing

$$\hat{H}_k^{\mathrm{TB}\,(r,i)} = Y_k^{(r)}\big(S_k^{\mathrm{TB}\,(i)}\big)^*/\big|S_k^{\mathrm{TB}\,(i)}\big|^2. \tag{6}$$

Alternatively, we can implement a decision-directed (DD) channel estimation approach where symbols decisions $\{\hat{S}_k^{(i)};\ k = 0, 1, \ldots, N-1\}$ are used.

C. CHANNEL ESTIMATION WITH DECISIONS

For the DD estimation of the CFR we do

$$\hat{H}_k^{\mathrm{DD}\,(r,i)} = Y_k^{(r,i)}\big(\hat{S}_k^{(i)}\big)^*/\big|\hat{S}_k^{(i)}\big|^2, \tag{7}$$

where $Y_k^{(r,i)} = Y_k^{(r)} - Y_k^{\mathrm{I}\,(r,i)}$ is the signal at the rth receive antenna with all signals but the one associated with Tx_i removed. Clearly, $Y_k^{\mathrm{I}\,(r,i)}$ is the interfering signal and

$$Y_k^{\mathrm{I}\,(r,i)} = \sum_{\substack{i'=1\\ i'\neq i}}^{M} H_k^{(r,i')} S_k^{(i)}. \tag{8}$$

Notice that, although we have written (8) using the true CFR, $\{H_k^{(r,i)};\ k = 0, 1, \ldots, N-1\}$, and transmitted symbols, $\{S_k^{(i)};\ k = 0, 1, \ldots, N-1\}$, in practice these values are not available to the receiver. Thus, we use estimates $\hat{H}_k^{\mathrm{EKF}\,(r,i)}$ (or for the first data symbol $\hat{H}_k^{\mathrm{TB}\,(r,i)}$) resulting

$$\hat{Y}_k^{\mathrm{I}\,(r,i)} = \sum_{\substack{i'=1\\ i'\neq i}}^{M} \hat{H}_k^{\{\mathrm{EKF},\mathrm{TB}\}\,(r,i')} \hat{S}_k^{(i)}. \tag{9}$$

where the computation of $\hat{H}_k^{\mathrm{EKF}\,(r,i)}$ is described in Sec. IV-B, and $\hat{H}_k^{\mathrm{TB}\,(r,i)}$ is given by (6).

D. CHANNEL EQUALIZATION

Consider the column vector $\mathbf{Y}_k = [Y_k^{(1)} \cdots Y_k^{(R)}]^\top$ associated with the received signals in the frequency-domain $\{Y_k^{(r)};\ k = 0, 1, \ldots, N-1\}$. Then

$$\mathbf{Y}_k = \mathbf{H}_k\mathbf{S}_k + \mathbf{N}_k, \tag{10}$$

where $\mathbf{H}_k$ is the $(R \times M)$ channel matrix with the (r,i)th element given by $\{H_k^{(r,i)};\ k = 0, 1, \ldots, N-1\}$, $\mathbf{S}_k = [S_k^{(1)} \cdots S_k^{(M)}]^\top$ the column vector associated to the data symbols $\{S_k^{(i)};\ k = 0, 1, \ldots, N-1\}$, and $\mathbf{N}_k = [N_k^{(1)} \cdots N_k^{(R)}]^\top$ the column vector associated to the channel noise process $\{N_k^{(r)};\ k = 0, 1, \ldots, N-1\}$. For a linear minimum mean squared error (MMSE)-based receiver, the output of the equalizer, $\tilde{\mathbf{S}}_k = [\tilde{S}_k^{(1)} \cdots \tilde{S}_k^{(M)}]^\top$, is given by

$$\tilde{\mathbf{S}}_k = (\mathbf{H}_k\mathbf{H}_k^\dagger + \alpha\mathbf{I})^{-1}\mathbf{H}_k^\dagger\mathbf{Y}_k \tag{11}$$

where $\mathbf{I}$ is an appropriate identity matrix and $\alpha = E[|N_k^{(r)}|^2]/E[|X_k^{(i)}|^2]$, which is assumed identical for all values of r and i. For the zero-forcing (ZF) receiver we have $\alpha = 0$. The computation of (11) requires, for each kth subcarrier, the inversion of a matrix which, depending on the number of antennas, can be very large.

IV. DOPPLER FREQUENCY SHIFT TRACKING

The state-space approach for tracking the Doppler frequency shift is formulated in this section. Particularly, we define an extended Kalman filter (EKF) [34] in terms of its process, and observation models. The process (or state-transition) model captures the rules governing the state dynamics, and the observation model the state observation, where the state is only partially observed. Notably, the definition of the process model (Sec. IV-A1) and observation model (Sec. IV-A2) are specific to the particular setup we are considering (i.e., multiple transmitters, MIMO receivers, and the channel model (3)), and are these steps that introduce novelty in our approach. After properly framing the problem as a state-space estimation problem through the definition of the process model and observation model, all the other steps (from Sec. IV-A3 to Sec. IV-A7) follow naturally.

A. THE EKF FOR TRACKING THE DOPPLER FREQUENCY SHIFT

1) PROCESS MODEL

Assuming that the state vector is $\mathbf{x}_l = [\boldsymbol{\nu}^\top\ \boldsymbol{\varphi}_l^\top]^\top$, where $\boldsymbol{\nu} = [f_D^{(1)}\Delta T\ \cdots f_D^{(M)}\Delta T]^\top$, and $\boldsymbol{\varphi}_l = [\varphi_l^{(1,1)}\ \cdots\ \varphi_l^{(R,M)}]^\top$, then the state-transition equation is

$$\mathbf{x}_{l+1} = \mathbf{F}\mathbf{x}_l, \tag{12}$$

where we introduce the subscript l denoting the snapshot instant, and where $\mathbf{F}$ is the state-transition matrix

$$\mathbf{F} = \begin{bmatrix} \mathbf{I}_M & \mathbf{0}_{M\times RM} \\ 2\pi\mathbf{I}_M \otimes \mathbf{1}_R & \mathbf{I}_{RM} \end{bmatrix}. \tag{13}$$

2) OBSERVATION MODEL

Consider the observations to be the real and imaginary parts of the modulo one complex exponential $\alpha_l^{(i)}/|\alpha_0^{(i)}|$.

Defining

$$\mathbf{f}(\boldsymbol{\varphi}_l) = \left[[f_1(\boldsymbol{\varphi}_l)]^\top \; [f_2(\boldsymbol{\varphi}_l)]^\top \right]^\top, \tag{14}$$

with $f_1(\boldsymbol{\varphi}_l) = [\cos(\varphi_l^{(1,1)}) \cdots \cos(\varphi_l^{(R,M)})]^\top$ and, $f_2(\boldsymbol{\varphi}_l) = [\sin(\varphi_l^{(1,1)}) \cdots \sin(\varphi_l^{(R,M)})]^\top$ results for the observation $\mathbf{z}_l = [z_l^{(1,1)} \cdots z_l^{(R,M)}]^\top$,

$$\mathbf{z}_l = \mathbf{f}(\boldsymbol{\varphi}_l) + \mathbf{v}_l, \tag{15}$$

where $\mathbf{v}_l = [v_l^{(1,1)} \cdots v_l^{(R,M)}]^\top$ is the observation noise vector.

The covariance matrix of the observation noise is $\mathbf{R} = \frac{\sigma_v^2}{2}\mathbf{I}$, where σ_v^2 is the variance of the complex white Gaussian noise process $v_l^{(i)}$. We assume the elements of the noise vector to be independent and identically distributed (IID).

3) PREDICTION STAGE

The prediction stage corresponds to the computation of the *a priori* state-mean $\mathbf{x}_{l|l-1}$, and state-covariance $\mathbf{P}_{l|l-1}$, using the *a posteriori* state-mean $\mathbf{x}_{l-1|l-1}$, and state-covariance $\mathbf{P}_{l-1|l-1}$, obtained during the previous iteration of the filter:

$$\mathbf{x}_{l|l-1} = \mathbf{F}\mathbf{x}_{l-1|l-1} \tag{16}$$

$$\mathbf{P}_{l|l-1} = \mathbf{F}\mathbf{P}_{l-1|l-1}\mathbf{F}^\top \tag{17}$$

4) FILTERING STAGE

The filtering stage is when the *a priori* state-mean $\mathbf{x}_{l|l-1}$ is combined with the information on the observation, resulting in a refined state estimate. Particularly, it corresponds to the computation of the *a posteriori* state-mean $\mathbf{x}_{l|l}$, and state-covariance matrix $\mathbf{P}_{l|l}$:

$$\mathbf{x}_{l|l} = \mathbf{x}_{l|l-1} + \mathbf{K}_l\mathbf{e}_l \tag{18}$$

$$\mathbf{P}_{l|l} = (\mathbf{I} - \mathbf{K}_l\mathbf{J}_{l|l-1})\mathbf{P}_{l|l-1} \tag{19}$$

where $\mathbf{e}_l$ is the so called residual, $\mathbf{K}_l$ the Kalman gain, and $\mathbf{J}_{l|l-1}$ the Jacobian of (14) evaluated w.r.t. the prediction state-mean $\mathbf{x}_{l|l-1}$, i.e.,

$$\mathbf{J}_{l|l-1} = \mathbf{J}(\mathbf{x}_l)|_{\mathbf{x}_l=\mathbf{x}_{l|l-1}}. \tag{20}$$

For the derivation of the Jacobian see Sec. IV-A7.

5) RESIDUAL

In (18), $\mathbf{e}_l$ corresponds to the measurement residual $\mathbf{z}_l - \mathbf{f}(\boldsymbol{\varphi}_{l|l-1})$. Clearly,

$$\mathbf{e}_l = \begin{bmatrix} \mathcal{R}\{\hat{\boldsymbol{\alpha}}_l\}/|\hat{\boldsymbol{\alpha}}_l| \\ \mathcal{I}\{\hat{\boldsymbol{\alpha}}_l\}/|\hat{\boldsymbol{\alpha}}_l| \end{bmatrix} - \begin{bmatrix} \cos(\boldsymbol{\varphi}_{l|l-1}) \\ \sin(\boldsymbol{\varphi}_{l|l-1}) \end{bmatrix}. \tag{21}$$

where $\hat{\boldsymbol{\alpha}}_l$ is the vector of the channel coefficient estimates $\hat{\boldsymbol{\alpha}}_l = [\hat{\alpha}_l^{(1)} \cdots \hat{\alpha}_l^{(M)}]$.

6) KALMAN GAIN

In (18), $\mathbf{K}_l$ is the Kalman gain

$$\mathbf{K}_l = \mathbf{P}_{l|l-1}\mathbf{J}_{l|l-1}\mathbf{S}_l^{-1}, \tag{22}$$

where $\mathbf{S}_l$ is the residual covariance matrix,

$$\mathbf{S}_l = \mathbf{R} + \mathbf{J}_{l|l-1}\mathbf{P}_{l|l-1}\mathbf{J}_{l|l-1}^\top. \tag{23}$$

7) JACOBIAN DERIVATION

The EKF is derived by approximating the nonlinear observation function (14) by the first term in its Taylor series expansion evaluated at the estimated state vector. The first term of the Taylor series corresponds to the Jacobian

$$\begin{aligned} \mathbf{J}(\mathbf{x}_l) &= \frac{\partial \mathbf{f}(\boldsymbol{\varphi}_l)}{\partial \mathbf{x}_l} \\ &= \begin{bmatrix} \frac{\partial f_1(\boldsymbol{\varphi}_l)}{\partial \nu} & \frac{\partial f_1(\boldsymbol{\varphi}_l)}{\partial \boldsymbol{\varphi}_l} \\ \frac{\partial f_2(\boldsymbol{\varphi}_l)}{\partial \boldsymbol{\nu}} & \frac{\partial f_2(\boldsymbol{\varphi}_l)}{\partial \boldsymbol{\varphi}_l} \end{bmatrix} \\ &= \begin{bmatrix} \mathbf{0}_M & [f_1'(\boldsymbol{\varphi}_l)]^\top \mathbf{I}_M \\ \mathbf{0}_M & [f_2'(\boldsymbol{\varphi}_l)]^\top \mathbf{I}_M \end{bmatrix} \end{aligned} \tag{24}$$

where $f_1'(\boldsymbol{\varphi}_l) = [-\sin(\varphi_l^{(1,1)}) \cdots - \sin(\varphi_l^{(R,M)})]^\top$, and $f_2'(\boldsymbol{\varphi}_l) = [\cos(\varphi_l^{(1,1)}) \cdots \cos(\varphi_l^{(R,M)})]^\top$.

B. EKF CFR ESTIMATE

The state estimate, $\hat{\mathbf{x}}_l$, results from the posterior state-mean (18) and it is used to produce an estimate $\hat{H}_{k,l}^{\text{EKF}\,(r,m)}$ of the CFR. In fact, using the elements of the state vector estimate $\hat{\mathbf{x}}_l = [\hat{\boldsymbol{\nu}}_l^\top \; \hat{\boldsymbol{\varphi}}_l^\top]^\top$. Particularly, $\hat{\boldsymbol{\nu}}_l = [\hat{f}_{D,l}^{(1)}\Delta T \cdots \hat{f}_{D,l}^{(M)}\Delta T]^\top$, and $\hat{\boldsymbol{\varphi}}_l = [\hat{\varphi}_l^{(1,1)} \cdots \hat{\varphi}_l^{(R,M)}]^\top$, we produce the estimate of the CIR

$$\hat{h}_{n,l}^{\text{EKF}\,(r,m)} = |\alpha_0^{(r,m)}|\delta(lT - \tau_m)\exp\left(j\hat{\varphi}_l^{(r,m)}\right). \tag{25}$$

Since we will be using the channel estimate obtained in the current time-slot, l, in the ensuing time-slot, $l+1$, we update (25) with the value of the Doppler shift obtained with the EKF, i.e.,

$$\begin{aligned} \hat{h}_{n,l+1}^{\text{EKF}\,(r,m)} &= |\alpha_0^{(r,m)}|\delta(lT - \tau_m) \\ &\quad \times \exp\left[j\left(\hat{\varphi}_l^{(r,m)} + 2\pi\hat{f}_{D,l}\Delta T\right)\right]. \end{aligned} \tag{26}$$

The estimated CFR results from applying the DFT to (26), i.e., $\{\hat{H}_{k,l}^{\text{EKF}\,(r,m)}; k = 0, 1, \ldots, N-1\} = \text{DFT}\{\hat{h}_{n,l}^{\text{EKF}\,(r,m)}; n = 0, 1, \ldots, N-1\}$ and later used in the channel equalization.

C. RECURSIVE BAYESIAN CRAMÉR-RAO BOUND

In order to determine the best performance achievable by the EKF we resort to the results of [35], where Tichavský *et al.* propose a recursive Bayesian Cramér-Rao bound (CRB). Accordingly, the recursion for the Fischer information matrix is

$$\mathbf{J}_{l+1} = \left(\mathbf{F}\mathbf{J}_l^{-1}\mathbf{F}^\top\right)^{-1} + \mathrm{E}_{\mathbf{x}_{l+1}}\left\{\mathbf{D}_{l+1}^\top\mathbf{R}_{l+1}^{-1}\mathbf{D}_{l+1}\right\}. \tag{27}$$

Defining,

$$\mathbf{J}_l = \begin{bmatrix} J_l^{\nu\nu} & J_l^{\nu\varphi} \\ J_l^{\nu\varphi} & J_l^{\varphi\varphi} \end{bmatrix}, \tag{28}$$

the first term on the right-hand-side of (27) is,

$$\left(\mathbf{F}\mathbf{J}_l^{-1}\mathbf{F}^\top\right)^{-1} = \begin{bmatrix} (2\pi)^2 J_l^{\varphi\varphi} - 4\pi J_l^{\nu\varphi} + J_l^{\nu\nu} & -2\pi J_l^{\varphi\varphi} + J_l^{\nu\varphi} \\ -2\pi J_l^{\varphi\varphi} + J_l^{\nu\varphi} & J_l^{\varphi\varphi} \end{bmatrix}. \tag{29}$$

Noting that matrix $\mathbf{D}_{l+1}$ is the Jacobian of the observation function (14) results for the 2nd term on the right-hand-side of (27),

$$\mathrm{E}_{\mathbf{x}_{l+1}}\left\{\mathbf{D}_{l+1}^\top \mathbf{R}_{l+1}^{-1} \mathbf{D}_{l+1}\right\} = \frac{2}{\sigma_v^2}\begin{bmatrix} 0 & 0 \\ 0 & 1 \end{bmatrix}. \tag{30}$$

Adding the two terms, (29), and (30), results in the following recursive expression,

$$\mathbf{J}_{l+1} = \begin{bmatrix} (2\pi)^2 J_l^{\varphi\varphi} - 4\pi J_l^{\nu\varphi} + J_l^{\nu\nu} & -2\pi J_l^{\varphi\varphi} + J_l^{\nu\varphi} \\ -2\pi J_l^{\varphi\varphi} + J_l^{\nu\varphi} & J_l^{\varphi\varphi} + \frac{2}{\sigma_v^2} \end{bmatrix}, \tag{31}$$

where the values used for $\mathbf{J}_0$ depend on the initialization conditions of the EKF [34].

Finally, we conclude this section by noting that the variance of the Doppler shift estimate, $\hat{\nu}_l$, and of the phase estimate, $\hat{\varphi}_l$, are lower bounded by the inverse of the Fischer information matrix elements $J_l^{\nu\nu}$, and $J_l^{\varphi\varphi}$, respectively, i.e.,

$$\mathrm{Var}(\hat{\nu}_l) > \left(J_l^{\nu\nu}\right)^{-1}, \tag{32}$$

$$\mathrm{Var}(\hat{\varphi}_l) > \left(J_l^{\varphi\varphi}\right)^{-1}. \tag{33}$$

V. PERFORMANCE RESULTS

In this section we present the performance results for the proposed solution. Unless stated otherwise, the values used in the simulations are those listed in Table 1. Particularly, we set each value in Table 1 with the scenario of space-to-space (or earth-to-space) communications in mind.

When considering a particular modulation order, we have to take into account the magnitude of the Doppler shifts, since larger modulation orders are significantly more sensitive to phase shifts that lower modulation orders. Since we are considering relatively large Doppler shifts, we selected QPSK modulations for robustness. Notably, QPSK is also the standard modulation scheme for satellite transmission [27, p. 88]. To keep the computational complexity of our simulations low, we set the FFT block size to 64, although our approach is suitable for any FFT block size. As for the number of data blocks, we set it to 100. This is a fairly large number and is selected so as to better illustrate the tracking performance of the EKF. Relatively to the minimum number of training blocks to be used in the initial estimation step, we set it to twice the number of transmitter satellites. A larger number of training blocks (e.g., four times the number of transmitter satellites), can be used and, eventually, could provide more precise estimates for the initial step obtained

TABLE 1. Simulation parameters.

Parameter	Value
Modulation	QPSK
FFT-size	$N = 64$ symbols
Number of data blocks	100 blocks
Number of training blocks	$2M$ blocks
Number of receiver antennas	$R = 4$ antennas
Number of transmitter satellites	$M = \{2, 3\}$ satellites
AoA separation	$\lvert\vartheta_i - \vartheta_{i'}\rvert > \frac{\pi}{5}$

TABLE 2. Maximum Doppler shifts for LEO orbits.

Altitude [km]	f_c [GHz]	$\lvert f_D^{\max}\rvert$ [kHz]	ΔT [ns]	$\lvert f_D^{\max}\rvert\Delta T$
600	2	48	1000	0.048
			520	0.025
			260	0.012
	20	480	260	0.125
			130	0.062
	30	720	260	0.187
			130	0.094
1500	2	48	1000	0.040
			520	0.021
			260	0.010
	20	480	260	0.104
			130	0.052
	30	720	260	0.156
			130	0.078

but this would come against what we are advocating with our work. Particularly regarding the use of overheads. As for the number of receiver antennas, we choose it to be 4. This number is selected so as to illustrate the MIMO scenario but other numbers could have been selected with similar results. Regarding the number of transmitter satellites, we consider in our simulations both the scenario with 2 and 3 satellites. These values are selected so as to illustrate ability of the proposed approach to cope with multiple Doppler shifts. Finally, the angle-of-arrival (AoA) separation was selected so as to provide enough diversity to separate the different sources.

For context, we list in Table 2 the maximum Doppler shifts for LEO orbits with different altitudes and carrier frequencies (see Table 5.3.4.3.2-7 of [4]) and compute the maximum normalized Doppler shifts assuming different values for the duration of the data block where each data block has $N = 64$ modulation symbols.

Fig. 4 depicts the BER performance for the proposed system with different normalized Doppler drifts $f_D \Delta T$, and $M = 2$ transmitter satellites. For reference, we also depict the BER curve for the case without Doppler shifts. Additionally, we included in our simulations the decision-feedback loop (DFL) proposed in [36]. Although being a mature technology, the DFL is the preferred approach to tackle the problem of synchronization in current operating communication systems [37], which makes it the natural choice with which to compare our proposal. Notice that, the BER curves depicted in the figure are computed taking the mean BER with respect to the first 100 data blocks, each with $N = 64$ QPSK symbols, and also the mean of the $M = 2$ links. By inspecting the figure we see that the EKF guarantees a BER performance close to the optimal, i.e., without Doppler, even when Doppler

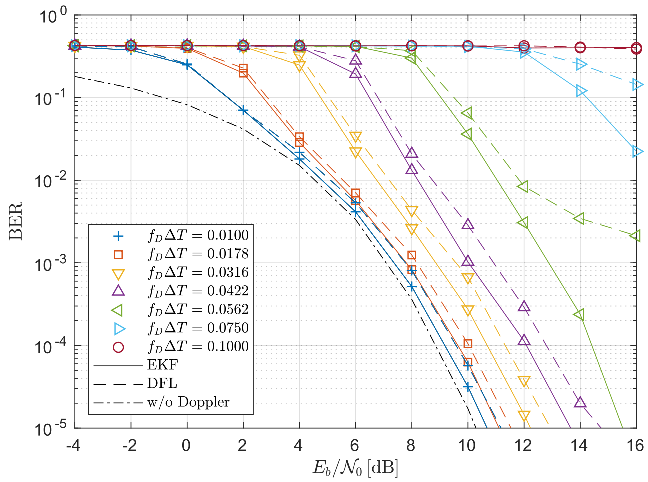

FIGURE 4. **BER performance for different Doppler drifts, and $M = 2$ transmitter satellites.**

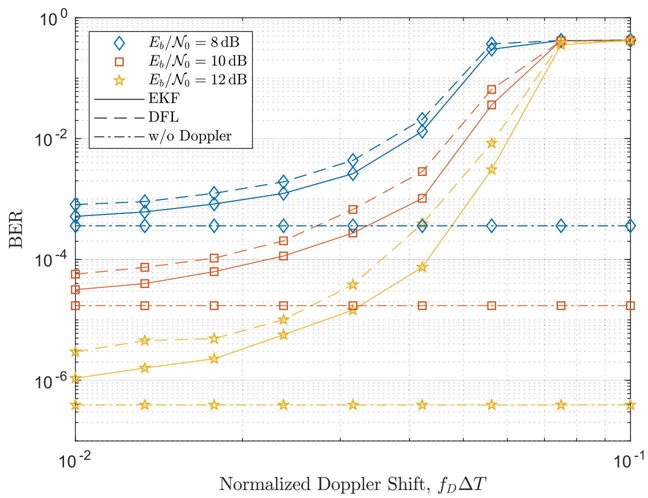

FIGURE 5. **BER *vs.* the normalized Doppler shift $f_D\Delta T$, and $M = 2$ transmitter satellites.**

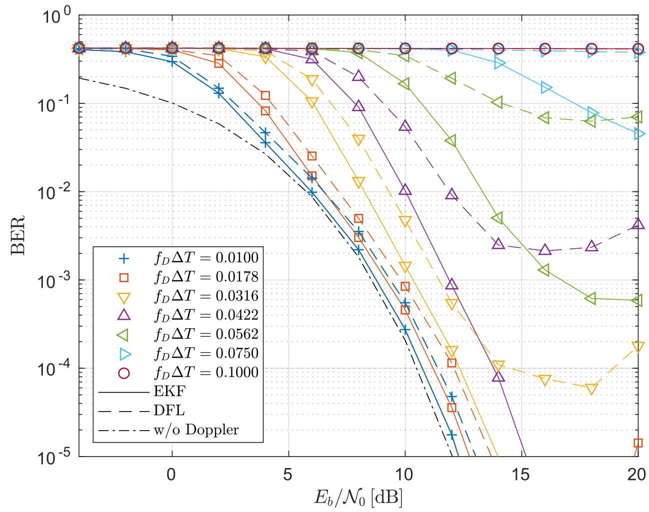

FIGURE 6. **BER performance for different Doppler drifts, and $M = 3$ transmitter satellites.**

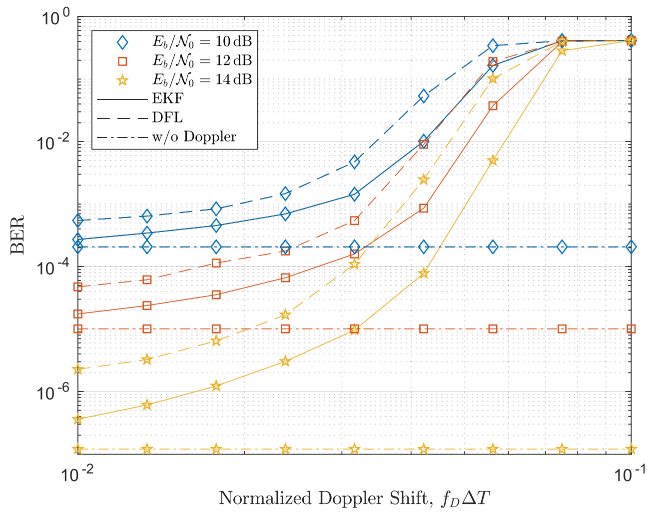

FIGURE 7. **BER *vs.* the normalized Doppler shift $f_D\Delta T$, and $M = 3$ transmitter satellites.**

is present. In fact, for a BER of 10^{-5} the loss relative to the optimal curve is less than 2 dB for $f_D\Delta T \leq 0.0316$. Notice that, the green dashed line, which is associated with the DFL and a normalized Doppler shift of $f_D\Delta T = 0.0562$, does not behave as the other curves, for which the BER drops steeply as we increase the $E_b/\mathcal{N}_0$, but holds on despite we increase the $E_b/\mathcal{N}_0$. This behavior is also visible in Fig. 6 for the dashed yellow, magenta, and green lines and the solid green line and results from the presence of the Doppler shift. In fact, what is happening in these cases is that the BER is no longer limited by channel noise (corresponding to the $E_b/\mathcal{N}_0$) but by the phase rotation induced on the signal constellation by the Doppler shift. For such values of the Doppler shift, the EKF (or the DFL) is no longer capable of tracking the Doppler drift properly and erroneous symbol decisions are produced at the receiver. Eventually, as we increase the Doppler further, the BER curves will became straight lines likes those associated to a normalized Doppler shift of $f_D\Delta T = 0.1$ in Fig. 4 and Fig. 6.

Fig. 5 depicts the BER *vs.* the normalized Doppler shift $f_D\Delta T$, and $M = 2$ transmitter satellites. By inspecting the figure we see that the EKF ensures a BER below 10^{-2} for $E_b/\mathcal{N}_0 = 8$ dB and $f_D\Delta T \leq 0.04$, or $E_b/\mathcal{N}_0 = 10$ dB and $f_D\Delta T \leq 0.05$. Similarly, we have BER $\leq 10^{-5}$ for $E_b/\mathcal{N}_0 = 12$ dB and $f_D\Delta T \leq 0.03$.

Fig. 6 depicts the BER performance for the proposed system with different normalized Doppler drift $f_D\Delta$, and $M = 3$ transmitter satellites. By inspecting the figure we can see that the EKF ensures a BER smaller that 10^{-4} for $E_b/\mathcal{N}_0 \geq 14$ dB even when $f_D\Delta T = 0.0422$.

Fig. 7 depicts the BER *vs.* the normalized Doppler shift $f_D\Delta T$, and $M = 3$ transmitter satellites. By inspecting the figure we see that the EKF ensures a BER smaller that 10^{-4} for $E_b/\mathcal{N}_0 = 14$ dB, and $f_D\Delta T \leq 3 \times 10^{-2}$.

Fig. 8 depicts the mean-squared error (MSE), and the CRB of the Doppler frequency estimate $\hat{f}_D\Delta T$. We consider a Doppler frequency shift $f_D\Delta T = 0.01$. Clearly, the EKF is capable of tracking effectively the Doppler shift, even with

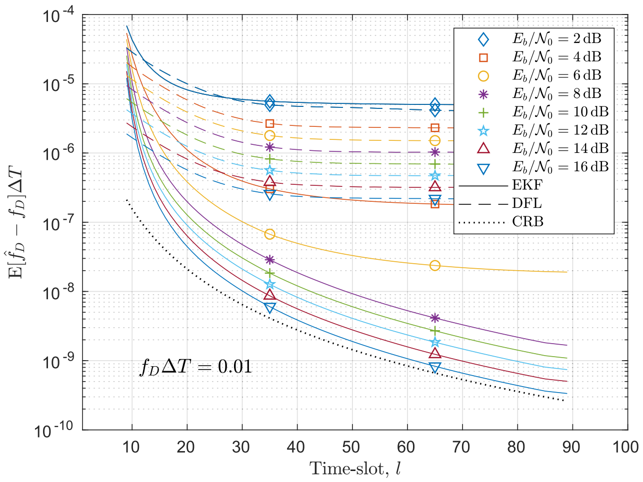

FIGURE 8. MSE and CRB for the estimate $\hat{f}_D\Delta T$.

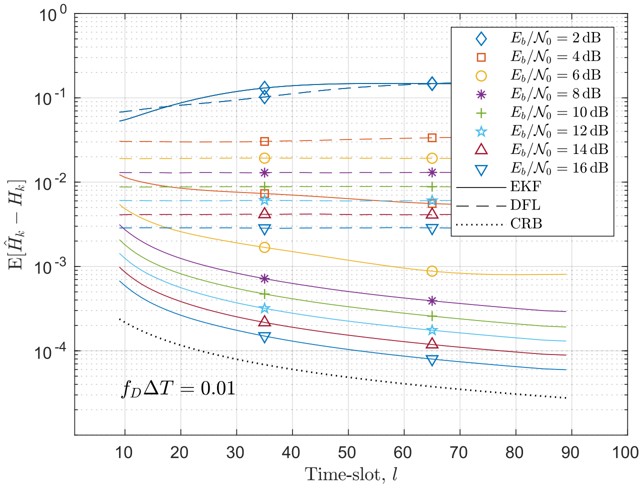

FIGURE 9. MSE and CRB for the estimate $\hat{H}_k$.

small values of $E_b/\mathcal{N}_0$ (e.g., with $E_b/\mathcal{N}_0 \geq 8$ dB we have a MSE of less than 10^{-8} for l greater than 50. Moreover, if the E_b/N_0 is sufficiently high then the MSE is close to the BCRB. Finally, although the DFL presents also a small MSE, the EKF is clearly superior.

Fig. 9 depicts the MSE, and the CRB of the CFR $\hat{H}_k$. We consider a Doppler frequency shift $f_D\Delta T = 0.01$. Clearly, the EKF is capable of tracking effectively the CFR, even with small values of $E_b/\mathcal{N}_0$ (e.g., with $E_b/\mathcal{N}_0 \geq 8$ dB we have a MSE of less than 10^{-3} for l greater than 30. Again, if the E_b/N_0 is sufficiently high then the MSE is close to the BCRB.

VI. CONCLUSION

In this paper we considered inter-satellite radio communications, where a multi-antenna receiving satellite is connected to several transmitting satellites. Associated with each transmitting satellite we can have substantially different Doppler shifts. We proposed a state-space approach for estimating the channels and track their variation, following the individual Doppler shift for each transmitting satellite. Our performance results indicate that the proposed channel tracking scheme is able to cope with high Doppler shifts, without the need for large channel estimation overheads. The proposed scheme may be fundamental for the communication systems of future satellite mega-constellations.

REFERENCES

[1] *Solutions for NR to Support Non-Terrestrial Networks (NTN)*, Standard TR 38.821 V16.0.0, 3GPP, Jan. 2020.

[2] *Study on Scenarios and Requirements for Next Generation Access Technologies*, TR 38.913 V16.0.0, 3GPP, Jul. 2020.

[3] *Study on Using Satellite Access in 5G; Stage 1*, Standard TR 22.822 V16.0.0, 3GPP, Jun. 2018.

[4] *Study on New Radio (NR) to Support Non-Terrestrial Networks*, TR 38.811 V15.4.0, 3GPP, Sep. 2020.

[5] Y. Turk and E. Zeydan, "Satellite backhauling for next generation cellular networks: Challenges and opportunities," *IEEE Commun. Mag.*, vol. 57, no. 12, pp. 52–57, Dec. 2019.

[6] G. Giambene, S. Kota, and P. Pillai, "Satellite-5G integration: A network perspective," *IEEE Netw.*, vol. 32, no. 5, pp. 25–31, Sep./Oct. 2018.

[7] O. Kodheli, "Satellite communications in the new space era: A survey and future challenges," *IEEE Commun. Surveys Tuts.*, vol. 23, no. 1, pp. 70–109, 4th Quart., 2021.

[8] I. Leyva-Mayorga, B. Soret, and P. Popovski, "Inter-plane inter-satellite connectivity in dense LEO constellations," *IEEE Trans. Wireless Commun.*, vol. 20, no. 6, pp. 3430–3443, Jun. 2021.

[9] R. Deng, B. Di, H. Zhang, L. Kuang, and L. Song, "Ultra-dense LEO satellite constellations: How many LEO satellites do we need?" *IEEE Trans. Wireless Commun.*, early access, Mar. 5, 2021, doi: 10.1109/TWC.2021.3062658.

[10] I. Leyva-Mayorga, B. Soret, M. Röper, D. Wübben, B. Matthiesen, A. Dekorsy, and P. Popovski, "LEO small-satellite constellations for 5G and beyond-5G communications," *IEEE Access*, vol. 8, pp. 184955–184964, 2020.

[11] Y. Su, Y. Liu, Y. Zhou, J. Yuan, H. Cao, and J. Shi, "Broadband LEO satellite communications: Architectures and key technologies," *IEEE Wireless Commun.*, vol. 26, no. 2, pp. 55–61, Apr. 2019.

[12] A. Guidotti, A. Vanelli-Coralli, M. Conti, S. Andrenacci, S. Chatzinotas, N. Maturo, B. Evans, A. Awoseyila, A. Ugolini, T. Foggi, L. Gaudio, N. Alagha, and S. Cioni, "Architectures and key technical challenges for 5G systems incorporating satellites," *IEEE Trans. Veh. Technol.*, vol. 68, no. 3, pp. 2624–2639, Mar. 2019.

[13] M. Katayama, A. Ogawa, and N. Morinaga, "Carrier synchronization under Doppler shift of the nongeostationary satellite communication systems," in *Proc. Singap. (ICCS/ISITA)*, Aug. 1992, pp. 466–470.

[14] I. Ali, N. Al-Dhahir, and J. E. Hershey, "Doppler characterization for LEO satellites," *IEEE Trans. Commun.*, vol. 46, no. 3, pp. 309–313, Mar. 1998.

[15] M.-H. You, S.-P. Lee, and Y. Han, "Adaptive compensation method using the prediction algorithm for the Doppler frequency shift in the LEO mobile satellite communication system," *ETRI J.*, vol. 22, no. 4, pp. 32–39, Dec. 2000.

[16] J. Lin, Z. Hou, Y. Zhou, L. Tian, and J. Shi, "Map estimation based on Doppler characterization in broadband and mobile LEO satellite communications," in *Proc. IEEE 83rd Veh. Technol. Conf. (VTC Spring)*, May 2016, pp. 1–5.

[17] A. A. Nasir, S. Durrani, H. Mehrpouyan, S. D. Blostein, and R. A. Kennedy, "Timing and carrier synchronization in wireless communication systems: A survey and classification of research in the last 5 years," *EURASIP J. Wireless Commun. Netw.*, vol. 2016, no. 1, p. 180, Dec. 2016.

[18] N. Hajiabdolrahim, S. R. Aghdam, and T. Eriksson, "An extended Kalman filter framework for joint phase noise, CFO and sampling time error estimation," in *Proc. IEEE 31st Annu. Int. Symp. Pers., Indoor Mobile Radio Commun.*, Aug. 2020, pp. 1–6.

[19] C. Zeng and W. Li, "Application of extended Kalman filter for tracking high dynamic GPS signal," in *Proc. IEEE Int. Conf. Signal Image Process. (ICSIP)*, Aug. 2016, pp. 503–507.

[20] X. Mao, M. Wada, and H. Hashimoto, "Nonlinear filtering algorithms for GPS using pseudorange and Doppler shift measurements," in *Proc. IEEE 5th Int. Conf. Intell. Transp. Syst.*, Sep. 2002, pp. 914–919.

[21] Z. Tu, T. Lu, and Q. Chen, "A novel carrier loop based on unscented Kalman filter methods for tracking high dynamic GPS signals," in *Proc. IEEE 18th Int. Conf. Commun. Technol. (ICCT)*, Oct. 2018, pp. 1007–1012.

[22] Z. Deng, L. Yin, L. Yang, and K. Liu, "The fine-interval tracking algorithm of GPS signal for high-speed spinning objects," in *Proc. 4th IEEE Int. Conf. Broadband Netw. Multimedia Technol.*, Oct. 2011, pp. 596–599.

[23] P. Savazzi and A. Vizziello, "Carrier synchronization in distributed MIMO satellite links," in *Proc. IEEE Int. Conf. Wireless Space Extreme Environ. (WiSEE)*, Dec. 2015, pp. 1–6.
[24] Y. Zhao, D. Tian, J. Tong, G. Cui, and W. Wang, "Carrier frequency synchronization algorithm for millimeter-wave inter-satellite links," in *Proc. IEEE 5th Int. Conf. Comput. Commun. (ICCC)*, Dec. 2019, pp. 843–847.
[25] D. Tian, Y. Zhao, J. Tong, G. Cui, and W. Wang, "Frequency offset estimation for 5G based LEO satellite communication systems," in *Proc. IEEE/CIC Int. Conf. Commun. China (ICCC)*, Aug. 2019, pp. 647–652.
[26] O. Popescu, "Power budgets for cubesat radios to support ground communications and inter-satellite links," *IEEE Access*, vol. 5, pp. 12618–12625, 2017.
[27] E. Lutz, M. Werner, and A. Jahn, *Satellite Systems for Personal and Broadband Communications*. Berlin, Germany: Springer, 2000.
[28] D. Castelain, C. Ciochina-Duchesne, J. Guillet, and F. Hasegwa, "SC-OFDM, a low-complexity technique for high performance satellite communications," in *Proc. 32nd AIAA Int. Commun. Satell. Syst. Conf.*, Aug. 2014, p. 4388.
[29] R. T. Schwarz, A. Knopp, and B. Lankl, "Performance of an SC-FDE SATCOM system in block-time-invariant orthogonal MIMO channels," in *Proc. IEEE Global Telecommun. Conf. (LOBECOM)*, Dec. 2011, pp. 1–6.
[30] *Satellite Earth Stations and Systems (SES); SC-FDMA Based Radio Waveform Technology for Ku/Ka Band Satellite Service*, Standard TR 103 297 V1.1.1, ETSI, Jul. 2017.
[31] R. T. Schwarz, T. Delamotte, K.-U. Storek, and A. Knopp, "MIMO applications for multibeam satellites," *IEEE Trans. Broadcast.*, vol. 65, no. 4, pp. 664–681, Dec. 2019.
[32] N. Benvenuto, R. Dinis, D. Falconer, and S. Tomasin, "Single carrier modulation with nonlinear frequency domain equalization: An idea whose time has come—Again," *Proc. IEEE*, vol. 98, no. 1, pp. 69–96, Jan. 2010.
[33] E. G. W. Peters, K. Day, and C. R. Benson, "A real-time Doppler compensating physical/data link layer protocol for satellite communications," in *Proc. IEEE Aerosp. Conf.*, Mar. 2020, pp. 1–11.
[34] H. L. van Trees, K. L. Bell, and Z. Tian, *Detection, Estimation, Filtering Theory—Part I: Detection, Estimation, Filtering Theory*, 2nd ed. Hoboken, NJ, USA: Wiley, 2013.
[35] P. Tichavsky, C. H. Muravchik, and A. Nehorai, "Posterior Cramer-Rao bounds for discrete-time nonlinear filtering," *IEEE Trans. Signal Process.*, vol. 46, no. 5, pp. 1386–1396, May 1998.
[36] P. O. Amblard, J. M. Brossier, and E. Moisan, "Phase tracking: What do we gain from optimality? Particle filtering versus phase-locked loops," *Signal Process.*, vol. 83, no. 1, pp. 151–167, Jan. 2003.
[37] H. Meyr and G. Ascheid, "Synchronization in digital communications. 1: Phase-, frequency-locked loops, and amplitude control," in *A Wiley-Interscience Publication*. New York, NY, USA: Wiley, 1990.

PEDRO PEDROSA was born in Luanda, Angola, in 1977. He received the M.Sc. and Ph.D. degrees in electrical and computer engineering from the Instituto Superior Técnico, Universidade de Lisboa, Lisbon, Portugal, in 2007 and 2012, respectively. From 2008 to 2014, he was a Research Fellow with the Instituto de Telecomunicações (IT), Lisbon. From Winter 2009 to Winter 2010, he was a Visiting Student with the OPERA Department, Université libre de Bruxelles (ULB). In 2014, he was a Research Fellow with the Laboratório de Pesquisas em Processamento Digital de Sinais, Universidade Federal de Santa Catarina (UFSC), Brazil, where he was a Visiting Professor of the Post-Graduation Program in electrical engineering at UFSC, from 2015 to 2016. Since 2018, he has been a Researcher with IT, Aveiro, Portugal. His research interests include within the broad fields of signal processing and digital communications.

DANIEL CASTANHEIRA received the Licenciatura (ISCED level 5) and Ph.D. degrees in electronics and telecommunications from the University of Aveiro, Aveiro, Portugal, in 2007 and 2012, respectively. He is currently an Auxiliary Researcher with the Instituto de Telecomunicações, Aveiro. He has been involved in several national and European Projects, namely RETIOT, SWING2, PURE-5GNET, HETCOP, COPWIN, PHOTON, within the FCT Portuguese National Scientific Foundation, and CODIV, FUTON and QOSMOS with the FP7 ICT. In 2011, he was with the "Departamento de Eletrônica, Telecomunicações e Informática," Aveiro University, as an Assistant Professor. His research interests include signal processing techniques for digital communications, with emphasis for physical layer issues including channel coding, precoding/equalization, and interference cancellation.

ADÃO SILVA received the M.Sc. and Ph.D. degrees in electronics and telecommunications from the Universidade de Aveiro, in 2002 and 2007, respectively. He is currently an Assistant Professor with the Department of Electronics, Telecommunications and Informatics, Universidade de Aveiro, and also a Senior Researcher with the Instituto de Telecomunicações. He has been participating in several national and European projects, namely the ASILUM, MATRICE, 4MORE within the ICT programme, and the FUTON and CODIV projects with the FP7 ICT. He has led several research projects, in the broadband wireless communications area, at the national level. He acted as a member of the TPC of several international conferences. His research interests include multiuser MIMO, multicarrier-based systems, cooperative networks, precoding, multiuser detection, massive MIMO, and millimeter wave communications.

RUI DINIS (Senior Member, IEEE) received the Ph.D. degree from the Instituto Superior Técnico (IST), Technical University of Lisbon, Portugal, in 2001, and the Habilitation degree in telecommunications from the Faculdade de Ciências e Tecnologia (FCT), Universidade Nova de Lisboa (UNL), in 2010. From 1992 to 2005, he was a Researcher with the Centro de Análise e Processamento de Sinal (CAPS), IST. From 2001 to 2008, he was a Professor with the IST. He is currently an Associate Professor with the FCT, UNL. Since 2003, he was an Invited Professor with Carleton University, Ottawa, ON, Canada. From 2005 to 2008, he was a Researcher with the Instituto de Sistemas e Robótica (ISR). Since 2009, he has been a Researcher with the Instituto de Telecomunicações (IT), UNL. He has been actively involved in several national and international research projects in the broadband wireless communications area. His research interests include transmission, estimation, and detection techniques. He is a VTS Distinguished Lecturer. He is or was an Editor of the IEEE Transactions on Wireless Communications, the IEEE Transactions on Communications, the IEEE Transactions on Vehicular Technology, the IEEE Open Journal on Communications Society, and *Physical Communication* (Elsevier). He was also a guest editor of several special issues.

ATÍLIO GAMEIRO received the Licenciatura and Ph.D. degrees from the University of Aveiro, Aveiro, Portugal, in 1985 and 1993, respectively. He is currently an Associate Professor with the Department of Electronics and Telecomunication, University of Aveiro, and a Researcher with the Instituto de Telecomunicações, Pólo de Aveiro, where he is the Head of group. He has authored or coauthored 200 technical articles in international journals and conferences. His industrial experience includes a period of one year with BT Labs and one year with NKT Elektronik. His main interests include signal processing techniques for digital communications and communication protocols, and within this research line he has done work for optical and mobile communications, either at the theoretical and experimental level. His current research interests include space-time-frequency algorithms for the broadband wireless systems and cross-layer design. He has been involved and has led IT or the University of Aveiro participation on more than 20 national and European projects.